Enhancing the Structural and Mechanical Properties of $Li_{1.22-X}Na_xMn_{0.78}O_2$ (0.00 ≤ X ≤ 0.05) by Doping with Sodium: DFT and FHI-Aims

N. Sithole[1*], K.M. Kgatwane[1] & P.E. Ngoepe[1]

ARTICLE INFO

Article details
Presented at the 26th annual conference of the Rapid Product Development Association of South Africa, held from 27 to 30 October 2025 in Pretoria, South Africa

Available online 8 Dec 2025

Contact details
* Corresponding author
njabulositholе500@gmail.com

Author affiliations
1 Materials Modelling Centre, University of Limpopo, South Africa

ORCID® identifiers
N. Sithole
https://orcid.org/0000-0002-5193-0828

K.M. Kgatwane
https://orcid.org/0009-0005-3124-7270

P.E. Ngoepe
https://orcid.org/0000-0003-0523-5602

DOI
http://dx.doi.org//10.7166/36-3-3348

ABSTRACT

The study examined the properties of Li-rich layered oxide cathode material, xLi_2MnO_3-(1-x)$LiMnO_2$, in an attempt to improve its electrochemical performance and capacity. The process included the Li-Na pair potentials. Using first-principles density functional theory (DFT) calculations to fit the Li-Na pair potentials, the mechanical and structural characteristics of the LiNaO structure were created as a model to fit the pair potentials. The calculated values of the lattice parameters had less than 2% difference, and the elastic constants of LiNaO were in good agreement with the experimental values of Na_2O. The elastic constants suggested that the LiNaO system was mechanically stable. The Buckingham pair potential parameters A and rho were fitted to the DFT pair potential and were found to be 28250.500 and 0.231 respectively. After refining the Buckingham potential parameters with the GULP code, the values of A and rho were 38500.500 and 0.177 respectively. The obtained Li-Na pair potentials were used in amorphisation and recrystallisation studies to determine the structural stability and mobility of lithium ions on the $Li_{1.22-x}Na_xMn_{0.78}O_2$ (x = 0.00, 0.01, and 0.05) nanoparticles using the DL_POLY molecular dynamics simulation package. We observed that <5% Na doping results in an ordered structure with regular cubic morphology and larger Li layer spacing, preventing the layered structure from turning into spinel.

OPSOMMING

Die studie het die eienskappe van Li-ryke gelaagde oksiedkatodemateriaal, xLi2MnO3-(1-x)LiMnO2, ondersoek in 'n poging om die elektrochemiese werkverrigting en kapasiteit daarvan te verbeter. Die proses het die Li-Na-paarpotensiale ingesluit. Deur gebruik te maak van eerste-beginsel digtheidsfunksionaalteorie (DFT) berekeninge om die Li-Na-paarpotensiale te pas, is die meganiese en strukturele eienskappe van die LiNaO-struktuur as 'n model geskep om by die paarpotensiale te pas. Die berekende waardes van die roosterparameters het minder as 2% verskil gehad, en die elastiese konstantes van LiNaO was in goeie ooreenstemming met die eksperimentele waardes van Na2O. Die elastiese konstantes het daarop gedui dat die LiNaO-stelsel meganies stabiel was. Die Buckingham-paarpotensiaalparameters A en rho is by die DFT-paarpotensiaal aangepas en is onderskeidelik 28250.500 en 0.231 gevind. Nadat die Buckingham-potensiaalparameters met die GULP-kode verfyn is, was die waardes van A en rho onderskeidelik 38500.500 en 0.177. Die verkrygde Li-Na-paarpotensiale is in amorfiserings- en herkristallisasiestudies gebruik om die strukturele stabiliteit en mobiliteit van litiumione op die Li1.22-xNaxMn0.78O2 (x = 0.00, 0.01 en 0.05) nanopartikels te bepaal deur die DL_POLY molekulêre dinamika-simulasiepakket te gebruik. Ons het waargeneem dat <5% Na-dotering lei tot 'n geordende struktuur met gereelde kubiese morfologie en groter Li-laagspasiëring, wat verhoed dat die gelaagde struktuur in spinel verander.

1. INTRODUCTION

To fulfil the increasing demand for consumer electronics, electric vehicles, and energy storage stations, lithium-ion (Li-ion) batteries with a high energy density and long lifespan are desperately needed. Currently, olivine $LiFePO_4$, spinel $LiMn_2O_4$, and layered Li [Co, Mn, Ni]O_2 oxides are the most widely used cathodes for Li-ion batteries; nevertheless, each has its pros and cons. Some of the disadvantages include poor capacity, low-rate capability, thermal instability, and high cost [1]. Lithium-rich layered oxides (LRLOs) do not contain cobalt, making them a viable alternative to cobalt-based cathodes. This feature makes LRLOs suitable for low-cost and environmentally friendly Li-ion batteries [2, 3]. This is because LRLOs offer a high theoretical energy density owing to the anionic redox activation, the affordability of earth-abundant Mn-rich compositions, and their extraordinarily high capacity. However, LRLO cathodes' frequent operating voltage degradation has restricted their commercialisation and practical use. In addition, the irreversible capacity loss during the first charge cycle, voltage fading, voltage hysteresis, low-rate performance, and poor cycling stability have all hindered LRLO's performance. In addition, because of the migration of the transition metal ions to the Li layers, it was discovered that both the Li_2MnO_3 and the $LiMO_2$ components transformed into the spinel phase, resulting in poor rate performance and considerable capacity fading. The amount and size of Li_2MnO_3 in the composites were also found to have an impact on their performance [4]. To enhance the electrochemical performance of various cathode materials, such as Li_2MnO_3, doping is the most used method to address the intrinsic instability of these materials. Although dopants will rarely use cationic lithium (Li) sites during electrode cycling, it is well known that this opportunity increases through intralayer or interlayer diffusion when the battery is operating normally. Two main factors make the study of electrochemical actuation in Li_2MnO_3 important: (i) upgrade the key arrangement first regarding the electrochemistry of cathode materials that include Mn^{4+}; and (ii) gather the necessary data to plan a possible class of "Li-rich" cathodes, of which Li_2MnO_3 is an essential component. Doping with alkaline elements, such as sodium (Na) or potassium (K), is a distinct approach that is currently being used. Alkali metals are crucial for enhancing the densification of commonly used electrolyte materials, which leads to improved ionic conductivity. These elements cannot replace either the oxygen anion or the transition-metal elements [1]. Rather, they replace Li because the monovalent ions Na^+ and K^+ can replace Li^+ without disrupting the Coulombic connection, making it easier for them to be inserted into the Li-slab [5]. To improve the segregation between the transition metal and the alkali ions, the current study focuses on partially substituting Na^+ ions for the mobile Li^+ ions. This is done by using the larger radius of the Na^+ cation (1.02 Å) compared with Li+ (0.76 Å) [5], and by improving the structural stability and Li diffusion kinetics' contribution to longer cycle life.

2. METHOD

We required lattice parameters and mechanical characteristics from a structure with Li and Na atoms to prepare to fit Li-Na Buckingham interatomic potentials. To create the LiNaO structure, we substituted half of the Na atoms in the Na_2O parent structure with lithium atoms. Using the CASTEP code, we optimised the geometry, performed k-point convergence and convergence tests for the cutoff energy on the LiNaO structure. The improved LiNaO structure was then used to calculate its mechanical properties. K-point mesh of 5x5x5 or 0.04 k-spacing and a kinetic energy cut-off of 700 eV were used in the CASTEP geometry optimisation of LiNaO.

2.1. Fritz Haber Institute ab initio materials simulations

Short-range repulsive potentials for both periodic and non-periodic systems were computed using Fritz Haber Institute ab initio materials simulations (FHI-AIMS). Two input files were needed for the calculator: control.in, which specifies the basis set and computational parameters; and the geometry.in atomic positions, crystal structure. In this case, we set the energy of two particles at a great distance – roughly 10 angstroms. With eV as the sole degree of freedom, the energy of two particles is shown as a component of the distance between molecules. Instead, we would rather assess an analytical equation [6]. By fitting a function to the data, we would obtain an analytical form. We carried out the regression for the Buckingham potential, which is a classic:

$$E(r) = A_{ij} \cdot e^{-\left(\frac{r}{p}\right)} - \frac{C_{ij}}{r^6}$$

where E(r) represents the potential energy between two atoms at a distance r. The parameter A is associated with the repulsive energy and is proportional to the exponential term. The parameter ρ relates to the steepness of the repulsive potential, while C is associated with the attractive (Van der Waal's) forces. Last, r denotes the distance between the two atoms. Since we worked on LiNaO, Buckingham's pair potential for the parent structure Na_2O, the objective of this study was to derive the interaction of Li-Na. A non-periodic structure was created consisting of Li and Na atoms using an atomic simulation environment (ASE). FHI-aims computed single-point energy at distances from 1.2 to 10 Å in increments of 0.125 Å, then subtracted the total energy obtained at 10 Å from all other total energies. A short-range repulsive graph of total energy versus Li-Na separation distance was constructed using the matplotlib library for visualisation.

2.2. Refining potentials with the general utility lattice program

Lattice parameters and elastic constants of the Li-Na interaction were calculated by setting variables in the general utility lattice program (GULP) input file using the interatomic potentials from FHI-aims and the constructed LiNaO parameters from CASTEP. To achieve the best results on both lattice parameters and elastic constants that matched well with the computed CASTEP mechanical characteristics, the potentials were changed using the known potentials from the parent structures.

2.3. Molecular dynamics

The DL_POLY code was used to perform all the molecular dynamics simulations [7]. The Li-Li, Li-O, O-O, Mn-Mn, Mn-O, Na-Na, and Na-O Buckingham potentials used in this study were derived from previous studies [8] along with the calculated Li-Na potentials. The MD simulations were performed using NVE at 50 ps simulation time for amorphisation and NVT ensembles at 12 ns simulation time for recrystallisation. Three supercells were created, starting with a pure structure of $Li_{1.22}Mn_{0.78}O_2$. Sodium was then introduced into the structure at two different concentrations, 1% and 5%, resulting in the formation of $Li_{1.21}Na_{0.01}Mn_{0.8}O_2$ and $Li_{1.17}Na_{0.05}Mn_{0.8}O_2$ respectively. The sodium dopant was randomly substituted in the structures of 44Å, each having 10800 atoms. Subsequently, these structures underwent a process of amorphisation at temperatures ranging from 1400 K to 2000 K, followed by recrystallisation from 1900 K to 1600 K, and finally annealing from 1700 K to 10 K.

3. RESULTS AND DISCUSSION

3.1. Structural and mechanical properties

The GGA-PBE functional was used to perform the DFT geometry optimisation on 70 LiNaO structures, each with a unique configuration of Na and Li. A cut-off energy of 700 eV and k-points of 5x5x5 were used in the calculations. The configuration that was found to be the most stable had the lowest energy of -7793.443 eV, and was used to perform mechanical properties calculations. The most stable LiNaO structure had lithium and sodium atoms occupying adjacent sodium sites, shown in Figure 1(c).

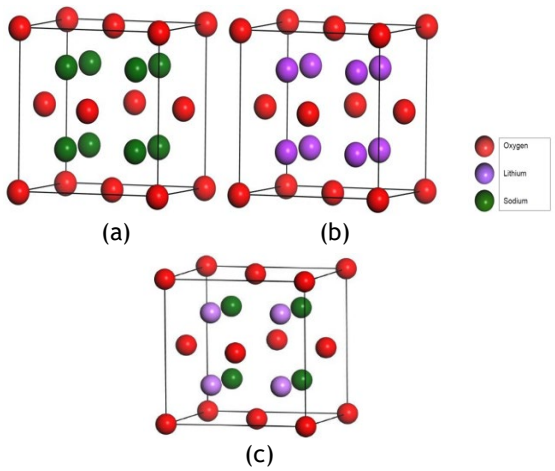

Figure 1: The unit cell of structures (a) Na_2O, (b) Li_2O, and the most stable unit cell of (c) LiNaO with a space group of $Fm\bar{3}m$

Table 1 compares the lattice parameters of the optimised LiNaO with those of the parent Na_2O structure. It shows a -7.37% decrease in lattice parameters *a* and *b*, and a -7.17% decrease in lattice parameter *c*. The lattice parameters of LiNaO were smaller than those of Na_2O because the ionic radius of lithium (0.76 Å) is less than that of sodium (1.02 Å), resulting in a size reduction. The LiNaO lattice parameters of a = b = 5.10 Å and c = 5.11 Å, shown in Table 3-1, lie in the range between those of Li_2O and Na_2O, and are in better agreement with those of the Na_2O structure compared with Li_2O.

Table 1: Lattice parameters of Exp Li_2O, Exp Na_2O, Na_2O and LiNaO

Lattice parameters (Å)	Li_2O Exp [9]	Exp [10]	Na_2O	LiNaO	%Diff vs Li_2O	%Diff vs Exp Na_2O
a	4.62	5.49	5.59	5.10	9.88	-7.37
b	4.62	5.49	5.59	5.10	9.88	-7.37
c	4.62	5.49	5.59	5.11	10.07	-7.17

DFT calculations on LiNaO using the generalised gradient approximation (GGA-PBE) were performed to obtain the mechanical properties shown in Table 2.

Table 2: Material properties of experimental Li_2O, Na_2O, and opt LiNaO

Elastic constants (GPa)	Li_2O Exp [9]	Na_2O Exp [10]	LiNaO
C_{11}	217	114.00	147.22
C_{12}	25	34.71	17.85
C_{44}	68	27.40	32.76
Bulk modulus	88.00	55.60	49.22

LiNaO has three independent elastic constants: C_{11}, C_{12}, and C_{44}. The elasticity in length is represented by C_{11}, while the elasticity in shape is represented by C_{12} and C_{44}. In general, we observed that C_{11} had the highest value, indicating that the length deformation was higher than the shape deformation. A key attribute for understanding and predicting stiffness and mechanical stability is hardness, as indicated by the C_{44} value. According to the present study, LiNaO exhibits superior shear elasticity to that of the experimental data of Na2O, confirming that replacing Na with Li has a greater effect on maintaining resistance to deformation. In contrast, LiNaO has a low bulk modulus and is thought to change volume easily, which is advantageous when deformation and significant pressure changes are required. Furthermore, mechanical stability can be used to determine crystal stability. The mechanical stability of a cubic structure must meet Born's requirements [11], as defined by the following elastic constant limitations: $C_{11} > 0$; $C_{44} > 0$; $C_{11} - C_{12} > 0$; $C_{11} + 2C_{12} > 0$.

Calculations:

$C_{11} > 0 = 147.22 > 0$

$C_{11} - C_{12} > 0 = 147.22 - 17.85 = 129.37 > 0$

$C_{11} + 2C_{12} > 0 = 147.22 + 2(17.85) > 0 = 182.92 > 0.$

$C_{44} > 0 = 32.76 > 0.$

Since all three stability requirements are met, LiNaO is mechanically stable. Experimentally, LiNaO's mechanical characteristics C_{11}, C_{12}, and C_{44} correspond well with those of Na_2O.

3.2. Derivation of interatomic potentials

3.2.1. Fitting the Li-Na Buckingham pair potential

In Figures 2(a) and (b), nlinfit and Scipy-optimisation (curve-fit) were used to fit the Buckingham potential parameters A_{ij} and ρ_{ij} to the pair potential obtained from DFT, while the value of C_{ij} was set to zero because the dispersion interactions were negligible in the short-range fitting range used. The 95% confidence intervals for A and rho were [18914.9856, 37585.9967] and [0.2287, 0.2341] respectively. In 2(d) the neural model approximates the expression for the total energy of the system and does not use the Buckingham equation. DL_POLY does not currently support the neural network potentials, known as machine-learned potentials.

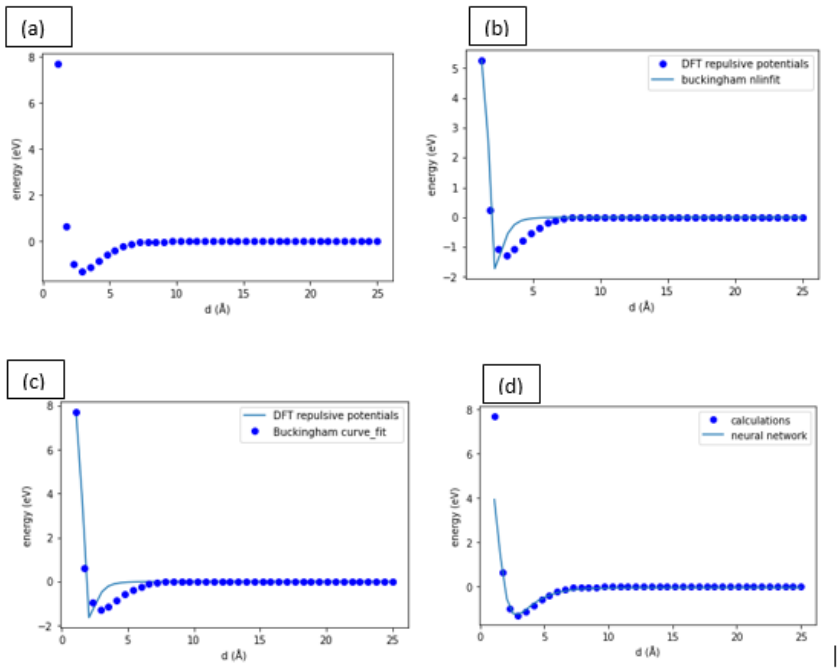

Figure 2: (a) Short-range pair potentials for the Li-Na obtained from FHI-aims DFT calculations. Fit of the Buckingham potential parameters using (b) nlinfit, (c) Scipy-optimisation (curve-fit), and (d) scikit-learn neural network regressor (artificial neural network)

3.2.2. Refinement of Li-Na Buckingham potential parameters

The FHI-aims results served as the foundation for fitting those potentials with the GULP code. A Fortran 90 algorithm was developed and used in conjunction with the GULP code to determine the parameters of Buckingham interatomic potentials within a given range to speed up the optimisation of correct potentials. The Buckingham potential parameters are presented in Table 3, along with the potentials optimised using the GULP algorithm, the DFT pair potential obtained from FHI-aims, and the known Li-Mn-O potentials listed in Table 6.

Table 3: Buckingham parameters of Li-Na using DFT and Li-Na GULP optimisation

	Li-Na interaction	
Buckingham parameters	**DTF pair potential**	**GULP**
A	28250.5	38500.5
P	0.231	0.177
C	0	0

In Table 4, the lattice parameters of the DFT pair potentials of Li-Na and CASTEP LiNaO are contrasted with those of the Li-Na GULP refined below. The data indicate that the lattice parameters *a* and *b* increased by 1.56%, whereas the lattice parameter *c* decreased by 1.58%. This was because of the defined potentials of Li-M-O and calculated Li-Na. A strong agreement existed between the optimised Li-Na GULP results and the LiNaO CASTEP results, validating the accuracy of the calculated pair potentials, thereby enabling better reproduction of Li/Na mobility, phase stability, and transformation pathways in MD simulations.

Table 4: Lattice parameters of DFT pair potential, CASTEP, and GULP

Lattice parameters	DFT pair potentials	CASTEP	GULP	% diff.
a* = *b	5.13	5.10	5.18	1.56
C	5.79	5.11	5.03	1.58

Table 5 compares the mechanical properties for C_{11}, C_{12}, and C_{44} of LiNaO and Na_2O based on the GULP-optimised structures, experimental data, and CASTEP DFT calculations. C_{44} demonstrated a lower value of enhanced compressibility for LiNaO under GULP optimisation, indicating that this material is less compressible to changes in volume when pressure is applied. Essentially, this means that LiNaO will not easily shrink or expand under varying pressure conditions. Furthermore, this characteristic suggests that the material is stiff and rigid, exhibiting strong intermolecular forces, as evidenced by its bulk modulus value of 57.910. The lattice constants and elastic constants closely matched those from first-principles DFT calculations. According to Born's criteria, we could conclude that LiNaO is mechanically stable.

Table 5: The elastic constants (GPa) for experimental Na_2O, LiNaO and Li-Na GULP structure

Mechanical properties	Exp Na_2O [10]	LiNaO CASTEP	GULP	% diff.
C_{11}	114.00	147.220	144.700	1.73
C_{12}	34.71	17.850	17.596	1.41
C_{44}	27.40	32.760	21.900	39.3
Bulk modulus	55.600	49.220	57.910	17.7

3.3. Molecular dynamics

The derived Buckingham pair potentials for Li-Na interaction, combined with the known potentials of $Li_{1.2-x}Na_xMn_{0.8}O_2$, were used in the 0.00%, 1.00%, and 5.00% doping of Na into $Li_{1.2-x}Na_xMn_{0.8}O_2$, and have been tested through molecular dynamics simulations. Molecular dynamics presents the results of the amorphisation and recrystallisation of $Li_{1.2-x}Na_xMn_{0.8}O_2$, calculated using the DL_POLY molecular dynamics simulation package. Analysis of the results was performed using diffusion coefficients.

Table 6: Buckingham potential parameters used to model Na-doped $Li_{1.2}Mn_{0.8}O_2$

Interaction	A (eV)	ρ (Å)	C (eV Å6)	Charge (Qij)
Mn^{4+} - Mn^{4+}	33883.9200	0.1560	16.0000	2.20
Mn^{4+} - Mn^{3+}	28707.2100	0.1560	16.0000	
Mn^{4+} - O	18645.8400	0.1950	22.0000	
Li - Li	270000.0000	0.1430	00.0000	0.55
Li - O	30000.0000	0.1542	00.0000	
Mn^{3+} - Mn^{3+}	23530.5000	0.1560	16.0000	1.65
Mn^{3+} - O	15538.2000	0.1950	22.0000	
O - O	11782.7600	0.2340	30.2200	-1.10
Na - O	29000.0000	0.1900	00.0000	
Na - Na	64500.0000	0.1900	00.0000	0.55
Li - Na	38500.5000	0.1770	00.0000	

The simulation temperature was varied from 1400 K to 2000 K in increments of 100 K, using a timestep of 0.001 picoseconds and 50 000 simulation steps. The NVE ensemble was used in the amorphisation calculations. We found that our systems start to amorphise from 1600 K, and were completely amorphised from 1700 K. The structure at 1800 K was sufficiently amorphised and was selected for the recrystallisation phase. The NVT ensemble was then used to carry out a recrystallisation calculation for 4 000 000 simulation steps, equilibration of 25% at a temperature of 1700 K. The recrystallisation process was followed by the cooling process at temperatures of 1300 K, 800 K, 300 K, and 10 K. A timestep of 0.003 picoseconds and 100 000 steps with an equilibration of 25% steps were used.

The $Li_{1.22-x}Na_xMn_{0.78}O_2$ supercell system is shown in Figure 3 at 10 K, 1700 K, and 1800 K respectively. Because of the temperature increase, the peaks in Figure 3(b) are not as distinct as those in Figure 3(a). In addition, there is a discernible difference between the temperatures of 10 K and 1700K, or between ~2.76Å and 10Å. The system is subjected to high temperatures, which scatter and transport the atoms across the structure. At 1800 K, the structure is in an amorphous form, suggesting that the system is totally amorphous and in a liquid phase.

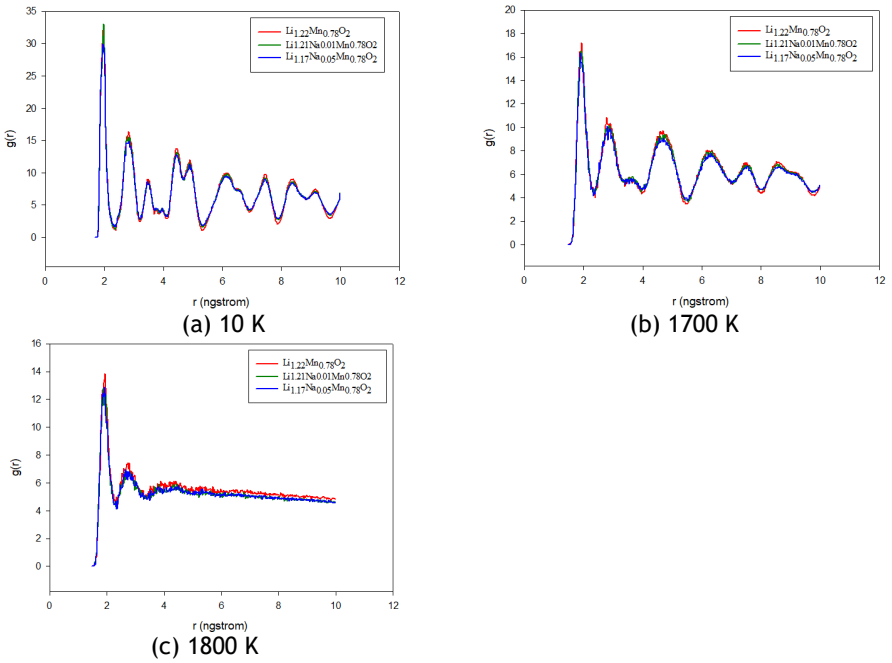

(a) 10 K (b) 1700 K

(c) 1800 K

Figure 3: Radial distribution function (RDF) for $Li_{1.22-x}Na_xMn_{0.78}O_2$ (0.00 ≤ x ≤0.05) nanoparticle

3.4. Diffusion coefficients

Figure 4 shows the plots of the Li-ion diffusion coefficients for the following nanoparticles: $Li_{1.22}Mn_{0.78}O_2$ (0.00 % Na), $Li_{1.21}Na_{0.01}Mn_{0.78}O_2$ (1.00 % Na), and $Li_{1.17}Na_{0.05}Mn_{0.78}O_2$ (5.00 % Na). Na^+ doping widens the gaps between Li layers in materials, allowing Li^+ ions to move through them more easily. These materials show a nonlinear effect of Na on Li mobility, which appears to decrease at 5.00% concentrations but increases at low concentrations owing to the complex role that Na plays in altering the crystal structure of the system and creating defects that impede ion transport[2]. At low concentrations, Na disrupts the existing lattice by creating new channels, which increases Li mobility. Li-ion mobility is the highest in $Li_{1.22}Mn_{0.78}O_2$ up to a temperature of 1300 K, second highest in $Li_{1.21}Na_{0.01}Mn_{0.78}O_2$, and lowest in $Li_{1.17}Na_{0.05}Mn_{0.78}O_2$. However, from 1300 K to 1700k K, the nanostructure with 1% Na concentration showed the highest Li diffusivity, followed by 5% Na. This indicates that Li-ion mobility in the nanoparticles slowed down as more lithium ions were replaced by sodium ions. Above 1300 K, the Li-ion mobility in the undoped $Li_{1.22}Mn_{0.78}O_2$ nanoparticle was the lowest. We observed that the nanoparticle started to amorphise at around 1400 K, which may explain the discrepancies in the Li-ion mobility at temperatures above 1300 K. At a higher concentration of Na, the Na-O interaction forms a stronger bond compared with 1.00% because, during recrystallisation, the Na atoms have been observed moving to the surface of the structure, and they act as “pillars”, creating structural defects that obstruct the path for Li-ion movement, which is observed from temperatures > 600 K between Na – 1.00% and 5.00%.

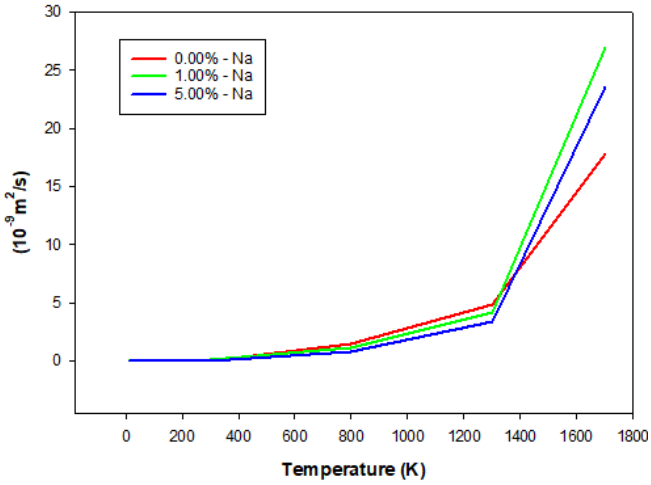

Figure 4: The diffusion coefficient plots for $Li_{1.22-x}Na_xMn_{0.78}O_2$ ($0.00 \leq x \leq 0.05$) for lithium ions in the temperature range of 10 K to 1700 K

4. CONCLUSION

The initial guess parameters of the Li-Na interatomic potential were calculated from the DFT repulsive potential and refined using GULP. In this study, we computed the properties of LiNaO to fit the Li-Na potential parameter using the DFT pair potential, as few experimental properties are available in the literature. LiNaO's mechanical and structural properties were deduced, and all the lattice parameters were confirmed to agree with the available experimental data. The obtained Li-Na Buckingham interatomic potential values, when combined with the known interatomic potentials for O-O, Li-O, Li-Li [8], Mn-O, and Mn-Mn [8], precisely reproduced the lattice parameters a and b, and c, of LiNaO to within 1.56% and 1.58% increase respectively. The elastic constants obtained were Li-Na adequate in comparison with their CASTEP values. $Li_{1.22-x}Na_xMn_{0.78}O_2$ (x = 0.00, 0.01, and 0.05) nanoparticles were successfully amorphised and recrystallised using the Li-Na Buckingham pair potential fitted in this study and the computed RDFs, which corroborate the success of the A + R. It has been demonstrated that doping $Li_{1.22-x}Na_xMn_{0.78}O_2$ with Na (0.00%–5.00%) enhances the structural and mechanical stability of the structure and inhibits the layered structure from turning into a spinel [5], which is in good agreement with previous research.

ACKNOWLEDGEMENTS

This study was carried out at the University of Limpopo. The authors thank Material Modelling Centre and Centre for High Performance Computing for lending them their computer resources so that the work that was presented could be completed.

Data availability: The corresponding author can provide the data reported in this paper on request.

Declaration: There are no conflicting interests disclosed by the authors.

Authors' contributions: Kenneth Kgatwane and Phuti Ngoepe came up with the paper's premise, while Kenneth Kgatwane handled the methodology and analysis. Draft preparation of the script, reviewing, and editing was by Beauty Shibiri, Phuti Ngoepe, and Kenneth Kgatwane. Every author has reviewed and approved the manuscript's final form.

REFERENCES

[1] **J.C. Knight and A. Manthiram**, "Effect of nickel oxidation state on the structural and electrochemical characteristics of lithium-rich layered oxide cathodes," *Journal of Materials Chemistry A*, vol. 3, no. 44, pp. 22199-22207, 2015. https://doi.org/10.1039/C5TA05703E

[2] **Y.H. Lou**, H.X Wei, L.B Tang, Y.D Huang, Z.Y Wang, Z.J He, C. Yan, J. Mao, K. Dai and J.C Zheng "Nickel-rich and cobalt-free layered oxide cathode materials for lithium-ion batteries," *Energy Storage Materials*, vol. 50, pp. 274-307, 2022. https://doi.org/10.1016/j.ensm.2022.05.019

[3] **L. Silvestri, A. Celeste, M. Tuccillo, and S. Brutti**, "Li-rich layered oxides: Structure and doping strategies to enable co-poor/co-free cathodes for Li-ion batteries," *Crystals*, vol. 13, no. 2, pp. 204, 2023. https://doi.org/10.3390/cryst13020204

[4] **C. Ghanty, R.N. Basu, and S.B. Majumder**, "Electrochemical characteristics of xLi_2MnO_3-(1-x)$Li(Mn_{0.375}Ni_{0.375}Co_{0.25})O_2$ ($0.0 \leq x \leq 1.0$) composite cathodes: Effect of particle and Li_2MnO_3 domain size," *ElectrochimicaActa*, vol. 132, pp. 472-482, 2014. https://doi.org/10.1016/j.electacta.2014.03.174

[5] **A.M. Hashem, A.E. Abdel-Ghany, R.S. El-Tawil, A. Mauger, and C.M. Julien**, "Effect of Na doping on the electrochemical performance of $Li_{1.2}Ni_{0.13}Co_{0.13}Mn_{0.54}O_2$ cathode for lithium-ion batteries," *Sustainable Chemistry*, vol. 3, no. 2, pp. 131-148, 2022. https://doi.org/10.3390/suschem3020010

[6] **V. Blum, S. Kokkott, and M. Rossi**. Matthias Scheffler and the FHI-aims team, with many contributors around the world, *All-electron electronic structure theory with numeric atom-centered basis functions*, FHI-aims.org, Berlin, Germany, 2024. https://fhi-aims.org /uploads/documents/FHI-aims.250320.pdf

[7] **I.T. Todorov and W. Smith**, *The DL_POLY_4 user manual*,Warrington, Cheshire, UK: STFC Daresbury Laboratory, 2011. https://www.ehu.eus/sgi/ARCHIVOS/dlpoly_man.pdf

[8] **T.X. Sayle, P.E. Ngoepe, and D.C. Sayle**, "Generating structural distributions of atomistic models of Li_2O nanoparticles using simulated crystallisation," *Journal of Materials Chemistry*, vol. 20, pp. 10452-10458, 2010. https://doi.org/10.1039/C0JM01580F

[9] **A. Watanabe, G. Kobayashi, N. Matsui, M. Yonemura, A. Kubota, K. Suzuki, M. Hirayama, and R. Kanno**, "Ambient pressure synthesis and H−conductivity of $LaSrLiH_2O_2$," *Electrochemistry*, vol. 85, pp. 88-89, 2017. https://doi.org/10.5796/electrochemistry 85.88

[10] M.C. Masedi, P.E. Ngoepe and H.M. Sithole, "Beyond lithium-ion batteries: A computational study on Na-S and Na-O batteries," *IOP Conference Series: Materials Science and Engineering*, vol. 169, 012001, 2017. https://doi.org/10.1088/1757-899X/169/1/012001

[11] **M. Born, K. Huang** and L. Max "Dynamical theory of crystal lattices," *American Journal of Physics*, 23, p. 474, 1955. https://doi.org/10.1119/1.1934059

[12] **P. Vanaphuti, J. Chen, J. Cao, K. Bigham, B. Chen, L. Yang, H. Chen, and Y. Wang**, "Enhanced electrochemical performance of the lithium-manganese-rich cathode for Li-ion batteries with Na and F codoping," *ACS Applied Materials and Interfaces*, vol. 11, pp. 37842-37849, 2019. https://doi.org/10.1021/acsami.9b13838

[13] **M.M. Thackeray, S.H. Kang, C.S. Johnson, J.T. Vaughey, R. Benedek, and S.A. Hackney**, "Li_2MnO_3-stabilized $LiMO_2$ (M = Mn, Ni, Co) electrodes for lithium-ion batteries," *Journal of Materials Chemistry*, vol. 17, no. 30, pp. 3112-3125, 2007. https://doi.org/10.1039/B702425H